ACS Catalysis

Research Article

Cite This: ACS Catal. 2018, 8, 7068−7076

pubs.acs.org/acscatalysis

Buffer-Induced Acceleration and Inhibition in Polyoxometalate-Catalyzed Organophosphorus Ester Hydrolysis

Daniel L. Collins-Wildman,[†] Mooeung Kim,[†] Kevin P. Sullivan,[†] Anna M. Plonka,[§] Anatoly I. Frenkel,[§] Djamaladdin G. Musaev,[†,‡] and Craig L. Hill*[,†]

[†]Department of Chemistry and [‡]Cherry L. Emerson Center for Scientific Computation, Emory University, 1515 Dickey Drive, Atlanta, Georgia 30322, United States

[§]Department of Material Science and Chemical Engineering, Stony Brook University, Stony Brook, New York 11794, United States

Supporting Information

ABSTRACT: The Zr-containing polyoxometalates (POMs), including $(Et_2NH_2)_8\{[\alpha\text{-}PW_{11}O_{39}Zr(\mu\text{-}OH)(H_2O)]_2\}\cdot 7H_2O$ (**1**), effectively catalyze the hydrolysis of nerve agent simulants at near-neutral pH. Analogous Zr-containing heterogeneous systems are much-studied and effective nerve-agent hydrolysis catalysts, but due to their heterogeneous nature, it is very challenging to know the exact structure of the catalytic sites during turnover and to clarify at the molecular level the elementary mechanistic processes. Here, under homogeneous conditions, hydrolysis rates of the nerve-agent simulant methyl paraoxon catalyzed by **1** are examined as a function of pH, ionic strength, catalyst, and substrate concentrations. In addition, the specific effect of three commonly used buffers is examined, revealing that acetate functions as a co-catalyst, phosphate inhibits hydrolytic activity, and 2-(*N*-morpholino)ethanesulfonic acid (MES) has no effect on the hydrolysis rate. Spectroscopic (^{31}P nuclear magnetic resonance) and computational studies demonstrate how each of these buffers interacts with the catalyst and offer explanations of their impacts on the hydrolysis rates. The impact of the nerve-agent hydrolysis product, methyl phosphonic acid, is also examined, and it is shown to inhibit hydrolysis. These results will aid in the design of future Zr-based hydrolysis catalysts.

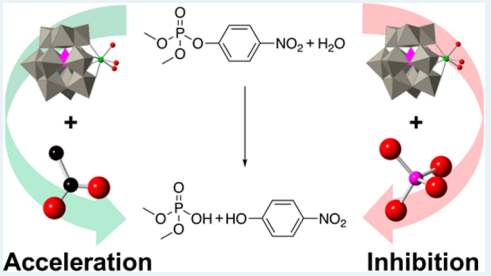

KEYWORDS: *polyoxometalate, hydrolysis, chemical warfare agents, buffer effects, co-catalysis, inhibition*

INTRODUCTION

The removal of toxic organophosphorus (OP) nerve agents and pesticides remains a significant and general goal. Ideally, this would be accomplished by materials that can either sequester or catalytically transform OP substances into nontoxic forms.[1−3] The primary route for decomposition of OP chemical-warfare agents (CWAs) is hydrolysis.[4] While strong bases can be used to hydrolyze and destroy large stockpiles of these nerve agents, the development of personal protective equipment requires a material, preferably a catalytic one, that can be integrated into masks and garments.[2,5]

Metal oxides, metal hydroxides, and metal organic frameworks (MOFs) have been studied extensively as potential materials for such protective equipment.[3,6−14] The Lewis acidic sites of these materials coordinate the phosphoryl (P═O) oxygen of the nerve agent and activate the phosphorus oxygen bond, making it more susceptible to nucleophilic attack and thereby accelerating the hydrolysis rate.[3] Recent studies have further interrogated the reactions of CWAs and simulants with MOF systems using synchrotron-based spectroscopic techniques (X-ray absorption near-edge structure, extended X-ray absorption fine structure, X-ray photoelectron spectroscopy, X-ray powder diffraction, and Raman spectroscopy) along with complementary computation.[15−17] Despite the use of these advanced methods, the heterogeneous nature of these materials continues to generate challenges in determining the exact mechanism of the reactions, including the nature of substrate and product interactions with the active site.

An in-depth understanding of the mechanism and governing factors of metal-catalyzed CWA decomposition is vital for optimizing catalyst performance. Therefore, the study of a molecular-metal-based Lewis acid catalyst would directly complement the existing body of research on heterogeneous hydrolysis catalysts. Techniques amenable to molecular systems, such as solution-phase nuclear magnetic resonance (NMR), would help facilitate the elucidation of mechanistic details of the CWA decontamination. One such compound is the zirconium containing polyoxometalate (POM), $(Et_2NH_2)_8[\{\alpha\text{-}PW_{11}O_{39}Zr(\mu\text{-}OH)(H_2O)\}_2]\cdot 7H_2O$ (**1**),[18] which is known to be an effective peptide and RNA hydrolysis catalyst.[19−24]

POMs are a class of highly modifiable, molecular transition-metal oxygen-anions that can function as oxidation, reduction, and hydrolysis catalysts.[25−33] They are capable of forming complexes with many elements across the periodic table[34] and can act as ligands for the strongly Lewis acidic metal ions

Received: January 29, 2018
Revised: June 14, 2018
Published: June 18, 2018

DOI: 10.1021/acscatal.8b00394
ACS Catal. 2018, 8, 7068−7076

including Zr(IV)[18,35−37] and Ce(IV).[38] Over the past decade, Parac-Vogt and co-workers have studied the POM-catalyzed hydrolysis of a number of compounds, including polypeptides and organophosphate RNA analogues.[39−44] They have demonstrated that Lewis acidic metal centers, including Zr(IV), activate phosphorus−oxygen bonds and enhance the rate of phosphate hydrolysis.[41] In addition, they have thoroughly examined several factors that affect the hydrolysis of organophosphorus compounds including ionic strength, pH, temperature, and catalyst concentration.[19−21,41,42,45−47]

Given that most nerve-agent hydrolysis products, such as methylphosphonic acid (MPA), are acidic and that hydrolysis is an inherently pH-dependent process, it is vital to have a buffer to maintain constant pH.[3,48,49] Furthermore, an analysis of the existing literature shows that the impact of buffers on the reaction outcome can be significant.[50−52] Herein, we report the considerable and diverse impact of common buffers on hydrolysis of the OP ester nerve-agent simulant, methyl-paraoxon or *O,O*-dimethyl *O*-(4-nitrophenyl) phosphate (DMNP) catalyzed by the Zr-POM, **1** (Scheme 1) and

Scheme 1. Hydrolysis of *O,O*-Dimethyl *O*-(4-Nitrophenyl) Phosphate (DMNP) in the Presence of the POM Catalyst 1

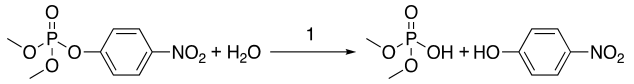

suggest a possible mechanism for the observed effects. This compound, **1**, was chosen as its speciation in solution has been well-characterized, and it is one of the most-active Zr-substituted POM hydrolysis catalysts. We report the specific effects of different buffer anions on Lewis acid catalyzed OP ester hydrolysis while carefully controlling the pH, ionic strength, catalyst concentration, and substrate concentration. Together, these results mark significant progress toward a full mechanistic understanding of homogeneous CWA hydrolysis by electrophilic zirconium centers and serve as insightful homogeneous models for heterogeneous Zr-based catalysts.

EXPERIMENTAL SECTION

Synthesis and Materials. The Zr-containing POM, $(Et_2NH_2)_{10}[Zr(\alpha\text{-}PW_{11}O_{39})_2]\cdot 7H_2O$ (**2**), was prepared by reacting a 2:1 molar ratio of $[\alpha\text{-}PW_{12}O_{40}]^{3-}$ with $ZrCl_2O\cdot 8H_2O$ in an aqueous Na_2CO_3 solution, followed by the addition of excess amounts of solid Et_2NH_2Cl as described in published procedures (detailed procedure described in the Supporting Information).[35] Similarly, $(Et_2NH_2)_8[\{\alpha\text{-}PW_{11}O_{39}Zr(\mu\text{−}OH)(H_2O)\}_2]\cdot 7H_2O$ (**1**) was prepared by reacting a 1:1 molar ratio of the in situ generated **2** with $ZrCl_2O\cdot 8H_2O$ in an aqueous HCl solution, followed by the addition of excess amounts of solid Et_2NH_2Cl, as described in the literature.[18,19] The monolacunary phosphotungstate, $K_7[\alpha\text{-}PW_{11}O_{39}]\cdot 14H_2O$, was prepared via a modified version of literature procedures (detailed procedure described in the Supporting Information).[53,54] All chemicals were of commercial quality unless otherwise specified.

Buffers were made by dissolving the desired concentration of acid in water, followed by adjustment to the desired pH by concentrated sodium hydroxide. This was done using volumetric glassware conducting the pH adjustment with most of the desired volume present before filling to the mark once the desired pH was reached. All pH measurements were done using an Orion 230A pH meter.

Characterization. Fourier transform infrared (FTIR) spectra were collected on a Nicolet 6700 FTIR spectrometer for samples **1** and **2** (Figures S1 and S2). Samples were prepared as KBr pellets using FTIR-grade KBr and 1−2% sample by weight. ^{31}P NMR spectra of **1** and **2** were collected on a Bruker 600 (Figures S3 and S4). Instead of running experiments in a deuterated solvent such as D_2O, NMR tube inserts filled with D_2O were added to each tube to maintain the lock throughout data acquisition and allow the pH of the solution to be precisely controlled. For speciation studies, POMs were dissolved and the pH adjusted, and the samples were then immediately taken to the NMR instrument for characterization. For each spectrum, 1024 scans were taken with a delay time of 2 s. Determination of phase purity of solid

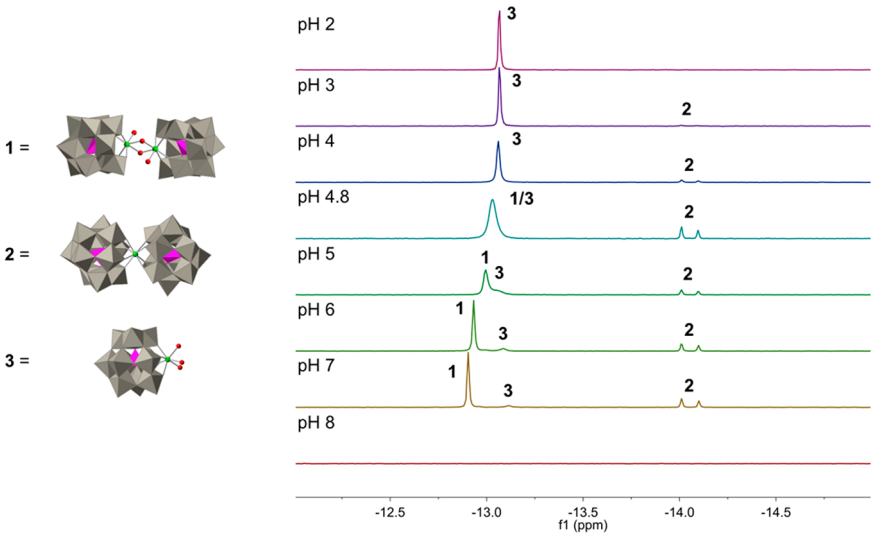

Figure 1. ^{31}P NMR of 2.5 mM **1** at varying pH values in deionized water. At pH 8, the lack of peaks for both **1** and **2** indicates they are unstable at this pH and have decomposed into other complexes not identified here. Solutions were pH adjusted with NaOH or $HClO_4$ (600 MHz NMR, 1024 scans, 85% H_3PO_4 internal standard). Polyhedral representations **1** and **2** are based on known crystal structures,[18,35] while **3** is a cartoon of the likely structure present in solution.

DOI: 10.1021/acscatal.8b00394
ACS Catal. 2018, 8, 7068−7076

samples of **1** was done using powder X-ray diffraction. The data were collected using a Rigaku Ultima-IV diffractometer equipped with Cu Kα radiation within a range of $5° \leq 2\theta \leq 40°$ (scanning rate: 1°/min). The unit cell parameters of ZrPOM were refined with LeBail fitting using the Jana2006 software, where peak shapes were refined with pseudo-Voigt function and peak asymmetry corrected with a Simpson function (Figure S7 and Table S1).[55] The background was modeled manually using 50 points.

Hydrolysis Studies. The pK_a of *p*-nitrophenol is 6.7, and when deprotonated, it exhibits a strong absorption band at 401 nm with an extinction coefficient of 18 380 $M^{-1}\cdot cm^{-1}$; in contrast, the protonated form is colorless.[56] Product formation during DMNP hydrolysis was therefore followed by measuring the strong absorption band of the hydrolysis product *p*-nitrophenolate on an Agilent 8453 UV−visible spectrophotometer. The initial rates were then determined from the slope of *p*-nitrophenolate formation versus time. Given that the reactions were conducted at pH values well below the pK_a of *p*-nitrophenol, small aliquots of the reaction solution were diluted by addition of 3 mL of pH 10, 0.45 M sodium borate buffer (greater detail is given in Supporting Information). This gave an appropriate concentration for absorption measurements and ensured that the product *p*-nitrophenol was well above its pK_a, yielding quantitative results. Full-reaction conversion was confirmed by ^{31}P NMR (Figure S8).

For all hydrolysis experiments, separate solutions of POM and DMNP were prepared and then combined to start the reaction. Reported concentrations are based on the combined volume of the two starting solutions. DMNP solutions were prepared at least 20 min prior to the start of the reaction because DMNP does not dissolve immediately in aqueous solution. During this time, negligible hydrolysis occurs as seen in the control reaction (Figure 1). The pH was adjusted after the dissolution of the POM but before the addition of DMNP to the solution, preventing product formation during pH adjustment. The timer was started upon addition of DMNP. The pH was measured again after the last absorption measurement was taken.

RESULTS AND DISCUSSION

Extensive studies by Parac-Vogt and co-workers on RNA analogue hydrolysis catalyzed by **1** established that there is a complex set of equilibria that govern the speciation of **1** in solution. This speciation is influenced by temperature, pH, ionic strength, catalyst concentration, and substrate concentration.[19−24] At high temperatures, ionic strength, and catalyst and substrate concentrations, **1** converts to **2** (Scheme 2, eq 1). In a second equilibrium process, **1** hydrolyzes to form two equivalents of the monomeric form $[\alpha\text{-}PW_{11}O_{39}Zr(OH)\text{-}(H_2O)_2]^{4-}$ (**3**) (Scheme 2, eq 2).

The pH dependence of this reaction can be monitored by ^{31}P NMR (Figure 1). Under acidic conditions, a single resonance is observed at −13.06 ppm, while at pH 7, there is a distinct chemical shift further down-field (−12.90). At pH 8, the POMs become unstable, and compounds **1**, **2**, and **3** decompose. At middle pH values (4−6), there are broadened peaks between these two resonances consistent with rates for equilibration that are comparable to the NMR time scale.[57] Previous diffusion-ordered spectroscopy (DOSY) NMR studies confirmed the existence of **3** below pH 4 and assigned **1** to the peak further down-field.[22] Given that **3** has multiple aqua ligands and is less sterically encumbered, it is expected to be more active than **1**. Compound **2** is coordinatively saturated, and it is therefore completely inactive.[24] Herein, knowledge of this speciation is used to inform experimental design. When **1** is used for subsequent experiments, the majority of which are at pH 4.8, it is assumed that the more active form, **3**, is both present and responsible for the majority of the catalytic activity. For pH values in which both **1** and **3** are present in solution, only one broadened peak at ∼−13 ppm is observed preventing quantification of the relative amounts of both species. Thus, for simplicity, apart from Figure 1, where the speciation is specifically examined, the ^{31}P NMR resonance at ∼−13 ppm is labeled as the more catalytically active species, **3**.

Scheme 2. Speciation of 1: Eq 1, Loss of Bridging Hydroxides and One Zirconium Center to Form the Eight-Coordinate Complex and 2; Eq 2, Hydrolysis of 1 to Form 3[a]

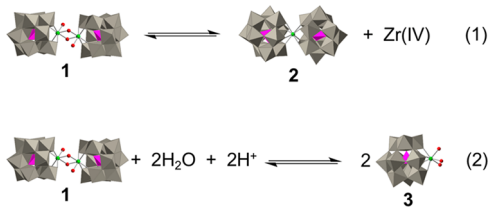

[a]This process is favorable at lower pH. WO_6, grey octahedra; PO_4, purple tetrahedra; Zr, green; O, red.

The activity of **1** was established by measuring the rate of hydrolysis of DMNP as a function of the concentration of **1** (Figure S9). The initial rates are close to linearly proportional to the starting concentration of **1**, indicating that the reaction is first-order in **1**. Any deviation likely results from the formation of **2** at higher concentrations of **1**.[20] Additionally, the acetic acid−acetate-buffered solution containing 6 mM of **1** hydrolyzes DMNP 96 times faster than the control (no catalyst in this buffer), indicating that **1**, as expected, is a DMNP hydrolysis catalyst. Full catalytic conversion of four equivalents of DMNP is achieved at pH 4.8 using a 0.5 M acetic acid−acetate buffer (Figure 2). Unbuffered control reactions show that equivalent concentrations of aqueous zirconium exhibit some activity, although substantially less than **1**, while the monolacunary Keggin, $K_7[\alpha\text{-}PW_{11}O_{39}]\cdot 14H_2O$, and counter-cation, Et_2NH_2, both having been independently evaluated,

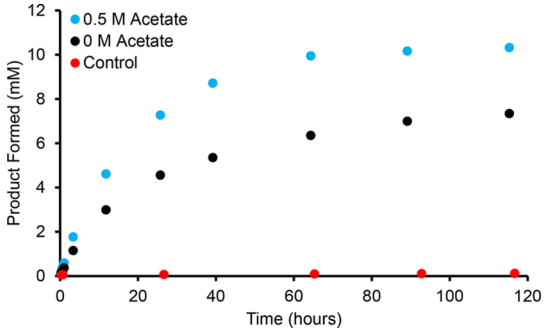

Figure 2. Product formation as a function of time for the full conversion of 10.3 mM DMNP. Conditions: pH 4.8, 10.3 mM DMNP, 2.5 mM **1** in the case of blue and black curves and 0 mM in the case of the red no-catalyst curve. An ionic strength was maintained at 0.3 M with 0.5 M acetic acid/acetate buffer (blue) or 0.3 M NaClO4 (black, red) with pH adjusted with NaOH.

DOI: 10.1021/acscatal.8b00394
ACS Catal. 2018, 8, 7068−7076

show negligible activity above the baseline hydrolysis rate (Table 1). Varying the concentration of DMNP also shows that the hydrolysis is first-order in this substrate (Figure S9).

Table 1. Initial Rates of Unbuffered Hydrolysis of 10.3 mM DMNP at pH 4.8 with No Additional Electrolyte Added and pH Adjusted with $HClO_4$ or NaOH

conditions	initial rate (nM/s)
2.5 mM **1**	286
DI water only	0.54
2.5 mM **2**	15
5 mM $K_7[\alpha\text{-}PW_{11}O_{39}]\cdot 14H_2O$	1.2
20 mM Et_2NH_2Cl	1.8
5 mM $ZrOCl_2$	119

Previous studies of organophosphate RNA analogue hydrolysis catalyzed by **1** have shown an initial rate dependence on the pH of the solution.[19−21] This pH dependence is particularly important because the hydrolysis product of DMNP, and nerve-agent hydrolysis products more broadly, are acidic. The solution pH drops in conjunction with reaction conversion, and the effect is more pronounced in non-buffered media near neutral pH. To test this dependence, the initial rates of DMNP hydrolysis were assessed over a range of pH values from 3 to 7 (Figure 3). This study was done without

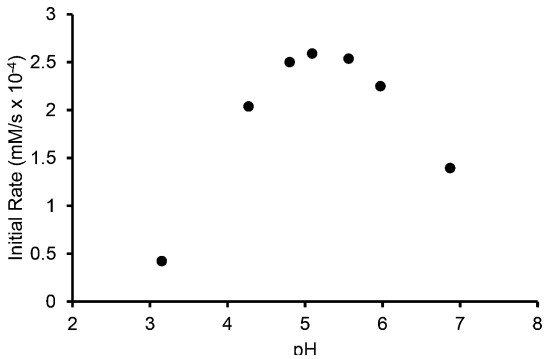

Figure 3. Initial rate dependence of DMNP hydrolysis on pH. Conditions: 2.5 mM **1**, 10.3 mM DMNP, pH adjusted with $HClO_4$ or NaOH.

the use of a buffer because no buffer can operate over such a broad range. For measurements of the initial rate, the pH drop from generation of acidic product is minimal.

Figure 3 shows that the initial rate maximizes at around pH 5; hence, further studies were conducted in this pH range. The decrease in rate at lower pH values can be attributed to the lack of a terminal hydroxide ligand on the zirconium center. Previous studies have shown that at lower pH, the predicted monomeric structure $[\alpha\text{-}PW_{11}O_{39}Zr(OH)(H_2O)_2]^{4-}$ becomes protonated, leaving only aqua ligands on the zirconium atom.[22] Because hydroxide is a better nucleophile, the reaction will proceed slower with water under the proposed mechanism for a single site catalyst.[3] At higher pH, the rate very likely decreases due to formation of the dimeric species, **1**, in solution, which also lacks a terminal hydroxide ligand and is more sterically hindered.[22]

Based on the pH dependence shown above and acidic nature of the hydrolysis product of DMNP, acetic acid−acetate at pH 4.8 was used to buffer many reactions in this study. Acetic acid has a pK_a of 4.76, which matches the pH window in which **1** has the highest activity. While buffering the solution is not essential for initial rate measurements, using a properly buffered solution allows a single system to be studied both at early times and under high-turnover conditions.

A 0.5 M solution of acetate buffer at pH 4.8 has a calculated ionic strength of 0.3 M.[58] Before examining catalysis under buffered conditions, the effect of ionic strength was also evaluated using sodium perchlorate, which does not interact with the POM. While maintaining a constant pH, increasing the concentration of $NaClO_4$ decreases the rate of catalytic hydrolysis (Figure 4). There are multiple explanations for this

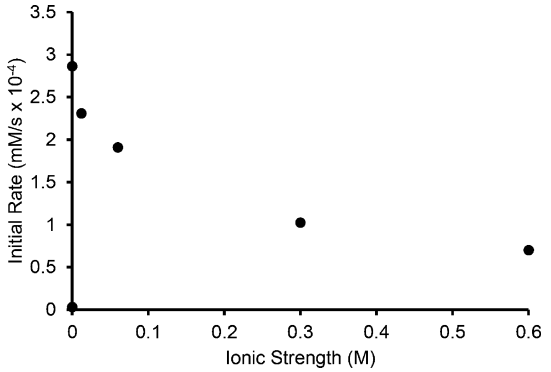

Figure 4. Initial rate dependence of DMNP hydrolysis on ionic strength. Higher ionic strength lowers the Coulombic attraction between the Zr(IV) center and partial negative on the phosphoryl oxygen, resulting in lower reactivity. Conditions: varied $[NaClO_4]$, 2.5 mM **1**, 10.3 mM DMNP, pH 4.8, pH adjusted with NaOH.

observed slowing of the reaction: first, high-ionic-strength favors the formation of the inactive species **2**; second, there will be a decreased interaction between the partial negative charge on the oxygen of DMNP and the Zr(IV) center in **3**; and third, the increased ionic strength appears to shift the monomer/dimer equilibrium in favor of the dimer, **1**, as indicated by the down-field shift of the ^{31}P NMR peak at ∼−13 ppm with increasing ionic strength (Figure S10). The NMR spectra also show that as the concentration of $NaClO_4$ increases from 0 to 0.3 M, the percentage of **2** increases from 12% at 0 M $NaClO_4$ to 20% at 0.3 M $NaClO_4$, which represents an 8% decrease in the active species. Interestingly, however, the initial rates drop from 2.9×10^{-4} to 1.0×10^{-4} M $\times$ s^{-1}, which represents a 66% rate decrease. This indicates that formation of **2** is not the sole cause of this rate loss. Instead, the weakened attractive force between the Zr-active site and DMNP or changes to the monomer and dimer equilibrium contribute to the rate decrease.

To account for effect of ionic strength, buffered and unbuffered catalytic reactions were compared while maintaining a constant ionic strength by adding the appropriate amount of $NaClO_4$. After 115 h, when the 0.5 M acetate buffered solution had reached 99% conversion of DMNP, the pH was recorded (Figure S11). As expected, the solution with the highest buffer concentration showed almost no change in pH, while the unbuffered solution dropped appreciably from pH 4.86 to 2.80. Significantly, however, the initial rates were not equal, with the initial rate increasing as a function of buffer concentration (Figure 5). To understand this phenomenon further, the impact of varying concentrations of acetate buffer in the reactions catalyzed by **1** was examined by ^{31}P NMR.

DOI: 10.1021/acscatal.8b00394
ACS Catal. 2018, 8, 7068−7076

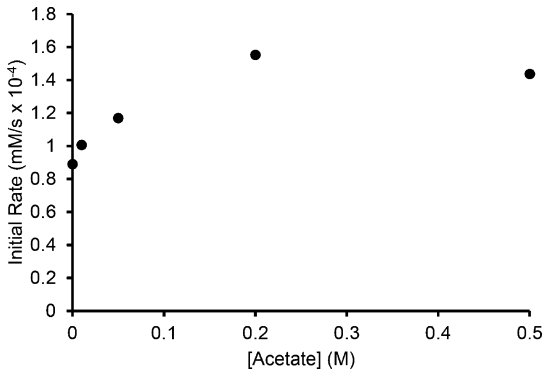

Figure 5. Initial rate dependence of DMNP hydrolysis on acetic acid/acetate buffer concentration. Conditions: buffer and $NaClO_4$ concentration varied; ionic strength, 0.3 M (combined effect of acetate and perchlorate ions), 2.5 mM **1**, 10.3 mM DMNP, pH 4.8, pH adjusted with NaOH.

The ^{31}P NMR spectra of **1** show a clear dependence on the acetate buffer concentration present in the solution (Figure 6). As the concentration of acetate increases, a new peak grows up-field of the original peak at −13.0 ppm, and the original peak begins to diminish. Both peaks shift up-field, concomitant with the increase in acetate concentration. The new peak eventually moves to −13.5 ppm. The formation of this peak is consistent with an acetate ion coordinating to the POM, either by displacing an aqua ligand coordinated to the Zr(IV) center creating a new Zr-acetate species or via hydrogen bonding with one of the zirconium-bound water molecules.

A pair of additional lines of evidence indicate that there is coordination between the POM and acetate. First, temperature-dependent ^{31}P NMR spectra were collected in 0.2 M acetic acid/acetate, such that both peaks are present in similar quantities (Figure 7). At elevated temperatures, the two peaks coalesce into a single peak indicative of a dynamic exchange process occurring at an intermediate rate relative to the NMR time scale.[57] Upon lowering of the temperature, the two peaks return to their original positions, demonstrating that the reversible change results from a dynamic equilibria rather than a physical change to the material. Second, POM-acetate coordination is further supported by changes to the ^{13}C NMR spectrum of an acetic acid−acetate buffer solution in the presence of **1** (Figure S12). The carboxylic acid carbon resonance observed at 178.52 in the absence of **1** shifts down-field to 178.64 and broadens from 1.8 to 5.4 Hz, again consistent with a dynamic exchange process. In contrast, the methyl carbon does not shift or broaden appreciably indicating the POM interaction is through the carboxylic acid group.

In contrast to the NMR resonances corresponding to **3**, the peaks at −14 ppm associated with catalytically inactive **2** do not shift as a function of acetate concentration. With 8 bonds, the Zr center in **2** is coordinatively saturated, leaving no open site for binding of an acetate ligand, and it does not have aqua ligands to facilitate hydrogen bonding. Accordingly, there is no chemical shift associated with increasing acetate concentration. To assess catalyst stability in the presence of acetate, ^{31}P NMR spectra were taken of samples aged in acetate buffer both with and without substrate (Figure S13). After 2 weeks, additional **2** forms; however, **3** remains the predominant species. In both the presence and absence of DMNP, **3** shows a similar decrease in concentration, suggesting that the presence of DMNP does not affect the speciation or stability of **3** appreciably

Based on the interactions between the buffer anion and POM, the observed dependence on the buffer concentration is more easily interpreted. This effect can be attributed to the acetate anion acting as a proximal base, making water a more-potent nucleophile,[59] or by helping facilitate proton transfer from water to the product in the transition state. In both cases, this would lower the barrier for product formation, increasing the reaction rate. To test this hypothesis, the pH dependence was re-examined while under buffered conditions. Given that the buffer capacity decreases to less than 10% of its maximum at 1 pH unit above or below the pK_a of the buffer, the effect of pH on the reaction rate was examined within the pH range of

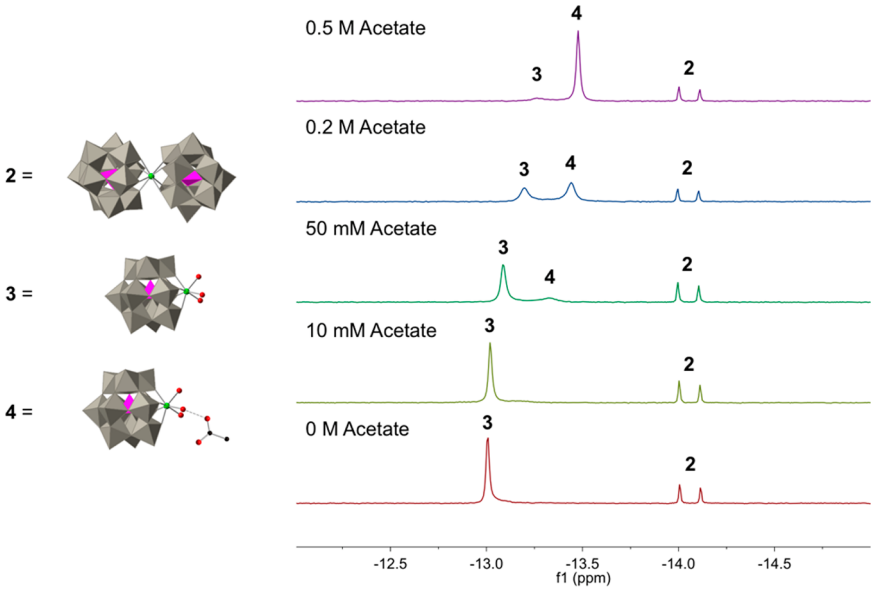

Figure 6. ^{31}P NMR spectra of 2.5 mM **1** at pH 4.8 with varying concentrations of acetate buffer. Solutions were pH-adjusted with NaOH and maintained at an ionic strength of 0.3 M with $NaClO_4$ (600 MHz NMR, 1024 scans, 85% H_3PO_4 internal standard). Polyhedral representation **2** is based on a known crystal structure,[35] while **3** and **4** are cartoons of the likely structures present in solution.

DOI: 10.1021/acscatal.8b00394
ACS Catal. 2018, 8, 7068−7076

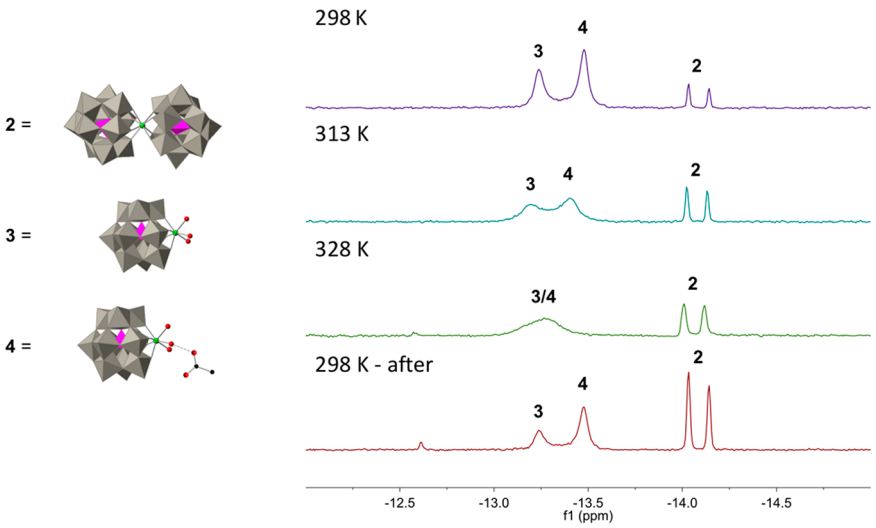

Figure 7. ^{31}P NMR spectra of a single solution of 2.5 mM **1** in 0.2 M acetic acid/acetate buffer at different temperatures (600 MHz NMR, 1024 scans, 85% H_3PO_4 internal standard). Spectra are presented in chronological order going from top to bottom. Note the increase in **2** in the last spectrum resulting from prolonged exposure to elevated temperatures used in the previous experiment. Polyhedral representation **2** is based on a known crystal structure,[35] while **3** and **4** are cartoons of the likely structures present in solution.

3.8 to 5.8. Unlike the unbuffered reaction, here, the reaction rate increased with increasing pH (Figure S14). This is likely because at the same concentration of buffer, there is a higher proportion of acetate anion present at higher pH that can act as a local base. In addition, the presence of acetate bound to zirconium could also affect the pH-dependent dimerization equilibrium, leading to an increased concentration of **3** at higher pH.

With these key findings for the effect of acetate buffer on catalytic hydrolysis by **1**, another buffer, phosphate, was examined because it is a common buffer for POM reactions in aqueous media and for hydrolysis reactions in general. While phosphate does not buffer at pH 4.8, experiments were carried out at this pH, nonetheless, to keep POM speciation constant. The ^{31}P NMR spectra show that, as with acetate, there is a chemical shift of the POM resonance up-field in the presence of phosphate indicating the formation of a complex with **3** (Figures S15 and S16). Additional evidence of complexation exists in the phosphate region of the spectrum where a new peak grows in the up-field of free phosphate as the POM concentration is increased. The peak is attributed to the phosphate molecules bound to the POM (Figure S17). In stark contrast with the acetate-buffered reactions, a solution with 0.3 M phosphate reduced the activity of the catalyst by a factor of 13 relative to 0.5 M acetic acid/acetate (Figures 8 and S18 and Table 2). A concentration of 0.3 M phosphate was used, as opposed to the 0.5 M used in the case of acetate, so that an ionic strength of 0.3 M would be maintained. This finding is consistent with a significantly different interaction mode of phosphate versus acetate with Zr(IV). It is likely that monobasic sodium phosphate competes with DMNP for binding to the zirconium center thus slowing reactivity, whereas acetate does not.

To support these experimental findings, density functional theory (DFT) computational studies were conducted. DFT studies (see the Supporting Information for details) provide clear insight into distinct binding modes and associated energetics of these two widely used buffers for hydrolysis reactions (Figure 9). The calculations predict that $H_2PO_4^-$ indeed does bind directly to the Zr center, which explains the

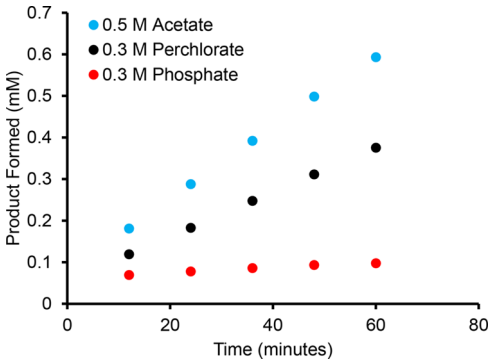

Figure 8. Product formation as a function of time in the presence of different anions. Acetate (blue) shows an enhancement over perchlorate (noncoordinating), whereas phosphate (red) exhibits inhibition. Conditions: ionic strength of 0.3 M, 2.5 mM **1**, 10.3 mM DMNP, pH 4.8, pH adjusted with NaOH.

Table 2. Initial Rates of Hydrolysis of 10.3 mM DMNP at pH 4.8 with an Ionic Strength of 0.3 M (Buffer or Electrolyte), with pH Adjusted with $HClO_4$ or NaOH

conditions	initial rate (nM/s)
0.3 M $NaClO_4$, 2.5 mM **1**	102
0.5 M acetate buffer, 2.5 mM **1**	144
0.5 M acetate buffer	3.2
0.3 M $NaH_2PO_4^-$, 2.5 mM **1**	11
0.3 M MPA, 2.5 mM **1**	19.7

loss of activity relative to non-nucleophilic and nonbasic ClO_4^-, which NMR spectra confirms does not interact strongly with the POM (Figure S10). In the case of acetate, the zirconium center remains open to substrate binding as acetate is predicted to bind in a noncompetitive mode to the POM by hydrogen bonding to a Zr-based aqua ligand. For comparison, direct coordination with the Zr center is higher in energy and, thus, less favorable (Figure S19).

The indirect binding mode of acetate to the catalytically active zirconium likely provides the hydrolysis rate enhancement via both proposed mechanisms described above: acting

DOI: 10.1021/acscatal.8b00394
ACS Catal. 2018, 8, 7068−7076

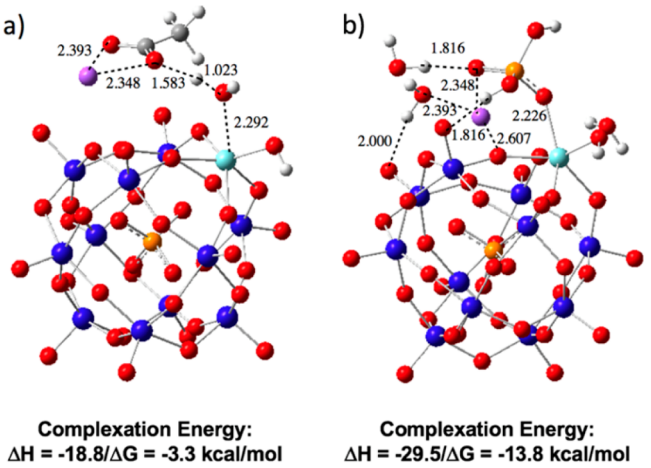

Figure 9. Comparison of the complexation energies and geometries between the POM monomer, **3**, and the anions (a) acetate and (b) phosphate. W, blue; O, red; Zr, blue-green; Na, purple; C, gray; P, orange; H, white.

as a local base and shifting the dimerization equilibrium in favor of the more active monomer. Figure 9a shows an increase in the O−H bond length of the aqua ligand hydrogen bonded to acetate. For this water molecule, one O−H bond distance is 0.969 Å, matching the typical length for a water O−H bond, while the second O−H bond has increased to 1.023 Å. This provides evidence that acetate, through hydrogen bonding with water, can act as a local base by pulling the hydrogen atom away from water, making it more hydroxide-like and, thus, a better nucleophile. Calculations suggest this occurs when the zirconium center in **3** has both a free coordination position and an aqua ligand (Figure S20).

Based on the above understanding of the interaction between **3** and $NaH_2PO_4^-$, a logical next step was to look at catalyst poisoning by the nerve agent hydrolysis product, MPA. Via ^{31}P NMR, we see that, as with both acetate and phosphate, the POM resonance shifts up-field in the presence of MPA (Figure S21). The initial rates of hydrolysis as a function of MPA show that, similar to phosphate, there is inhibition of the reaction (Figure S22). This suggests that the binding of MPA happens in competition with DMNP, significantly slowing the reaction.

In light of the large number of CWA hydrolysis studies involving *N*-ethylmorpholine (NEM) as a buffer,[7,9,10,13,49,60] the effect of a morpholine-based buffer was also examined here. The compound 2-(*N*-morpholino)ethanesulfonic acid (MES) was chosen as it is very similar in structure to NEM, but it has a lower pK_a of 6.16, allowing it to buffer at pH values at which both **1** and **3** will be present in solution. A pH of 5.8 was chosen to maximize both the concentration of **3** and deprotonated MES as a means to probe the effect of a local nucleophile and base in solution. Interestingly, the initial rate of hydrolysis was effectively independent of MES concentration while maintaining a constant ionic strength (Figure 10). The ^{31}P NMR shows that in the presence and absence of MES there is no change in the chemical shift of the POM, indicating that there is little or no interaction with MES (Figure S23). Thus, the MES is not involved in the rate-limiting step. Future studies will continue to examine other buffer molecules to further develop the relationship between buffer−catalyst interaction and observed hydrolysis chemistry.

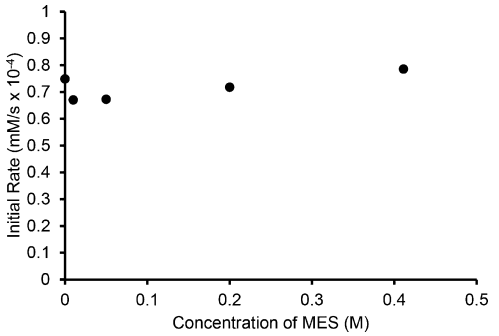

Figure 10. Initial rate dependence of DMNP hydrolysis as a function of MES concentration. Conditions: MES and $NaClO_4$ concentration varied; ionic strength, 0.3 M (combined effect of MES and perchlorate ions), 2.5 mM **1**, 10.3 mM DMNP, pH 5.8, pH adjusted with NaOH.

CONCLUSIONS

This is the first report of an electrophilic Zr-substituted POM catalytically hydrolyzing a CWA simulant at near-neutral pH. This study also reveals that buffer anions, often thought to be relatively innocent in CWA hydrolyses, can play key roles in such reactions by either accelerating (co-catalyzing) or inhibiting the rate. This effect results from their direct interaction with the catalyst in solution. Other buffer ions, such as MES, that are non-coordinating have no effect on the rate of hydrolysis. Future work will expand on this relationship between buffer-catalyst coordination and its impact on catalyzed hydrolysis rates. Lastly, the nerve agent hydrolysis product, methyl phosphonic acid (MPA), shows the inhibition of **1**-catalyzed hydrolyses. Because this POM has structural similarities to many of the Zr-based heterogeneous systems, which also experience similar product inhibition, this system provides a good means of probing and potentially studying the reversal of such inhibition. This will have important implications on the poisoning and long-term use of all Zr-based CWA hydrolysis catalysts.

ASSOCIATED CONTENT

Supporting Information

The Supporting Information is available free of charge on the ACS Publications website at DOI: 10.1021/acscatal.8b00394.

Additional details on experimental procedures, FTIR spectra, NMR spectra, powder X-ray diffraction data, initial rates data, reaction conversion profiles, and calculated Cartesian coordinates. (PDF)

AUTHOR INFORMATION

Corresponding Author

*E-mail: chill@emory.edu.

ORCID

Anna M. Plonka: 0000-0003-2606-0477
Anatoly I. Frenkel: 0000-0002-5451-1207
Djamaladdin G. Musaev: 0000-0003-1160-6131
Craig L. Hill: 0000-0002-5506-9588

Notes

The authors declare no competing financial interest.

DOI: 10.1021/acscatal.8b00394
ACS Catal. 2018, 8, 7068−7076

■ ACKNOWLEDGMENTS

The Bruker 600 NMR was funded by NSF grant no. CHE-1531620. We thank Natalie Uhlikova for calculating atom positions. We thank DTRA (ARO award no. W911NF-15-2-0107) for support. The authors gratefully acknowledge NSF MRI-R2 grant (CHE-0958205 for D.G.M.) and the use of the resources of the Cherry Emerson Center for Scientific Computation.

■ REFERENCES

(1) Yang, Y. C.; Baker, J. A.; Ward, J. R. Decontamination of chemical warfare agents. *Chem. Rev.* **1992**, *92*, 1729−1743.
(2) Smith, B. M. Catalytic methods for the destruction of chemical warfare agents under ambient conditions. *Chem. Soc. Rev.* **2008**, *37*, 470−478.
(3) Jang, Y. J.; Kim, K.; Tsay, O. G.; Atwood, D. A.; Churchill, D. G. Update 1 of: Destruction and Detection of Chemical Warfare Agents. *Chem. Rev.* **2015**, *115*, PR1−PR76.
(4) Kinnan, M. K.; Creasy, W. R.; Fullmer, L. B.; Schreuder-Gibson, H. L.; Nyman, M. Nerve Agent Degradation with Polyoxoniobates. *Eur. J. Inorg. Chem.* **2014**, *2014*, 2361−2367.
(5) López-Maya, E.; Montoro, C.; Rodríguez-Albelo, L. M.; Aznar Cervantes, S. D.; Lozano-Pérez, A. A.; Cenís, J. L.; Barea, E.; Navarro, J. A. R. Textile/Metal−Organic-Framework Composites as Self-Detoxifying Filters for Chemical-Warfare Agents. *Angew. Chem., Int. Ed.* **2015**, *54*, 6790−6794.
(6) DeCoste, J. B.; Peterson, G. W. Metal−Organic Frameworks for Air Purification of Toxic Chemicals. *Chem. Rev.* **2014**, *114*, 5695−5727.
(7) Katz, M. J.; Mondloch, J. E.; Totten, R. K.; Park, J. K.; Nguyen, S. T.; Farha, O. K.; Hupp, J. T. Simple and Compelling Biomimetic Metal−Organic Framework Catalyst for the Degradation of Nerve Agent Simulants. *Angew. Chem., Int. Ed.* **2014**, *53*, 497−501.
(8) Katz, M. J.; Moon, S.-Y.; Mondloch, J. E.; Beyzavi, M. H.; Stephenson, C. J.; Hupp, J. T.; Farha, O. K. Exploiting parameter space in MOFs: a 20-fold enhancement of phosphate-ester hydrolysis with UiO-66-NH_2. *Chem. Sci.* **2015**, *6*, 2286−2291.
(9) Mondloch, J. E.; Katz, M. J.; Isley Iii, W. C.; Ghosh, P.; Liao, P.; Bury, W.; Wagner, G. W.; Hall, M. G.; DeCoste, J. B.; Peterson, G. W.; Snurr, R. Q.; Cramer, C. J.; Hupp, J. T.; Farha, O. K. Destruction of chemical warfare agents using metal−organic frameworks. *Nat. Mater.* **2015**, *14*, 512−516.
(10) Moon, S.-Y.; Liu, Y.; Hupp, J. T.; Farha, O. K. Instantaneous Hydrolysis of Nerve-Agent Simulants with a Six-Connected Zirconium-Based Metal−Organic Framework. *Angew. Chem., Int. Ed.* **2015**, *54*, 6795−6799.
(11) Yang, D.; Bernales, V.; Islamoglu, T.; Farha, O. K.; Hupp, J. T.; Cramer, C. J.; Gagliardi, L.; Gates, B. C. Tuning the Surface Chemistry of Metal Organic Framework Nodes: Proton Topology of the Metal-Oxide-Like Zr6 Nodes of UiO-66 and NU-1000. *J. Am. Chem. Soc.* **2016**, *138*, 15189−15196.
(12) Moon, S.-Y.; Howarth, A. J.; Wang, T.; Vermeulen, N. A.; Hupp, J. T.; Farha, O. K. A visually detectable pH responsive zirconium metal-organic framework. *Chem. Commun.* **2016**, *52*, 3438−3441.
(13) Islamoglu, T.; Atilgan, A.; Moon, S.-Y.; Peterson, G. W.; DeCoste, J. B.; Hall, M.; Hupp, J. T.; Farha, O. K. Cerium(IV) vs Zirconium(IV) Based Metal−Organic Frameworks for Detoxification of a Nerve Agent. *Chem. Mater.* **2017**, *29*, 2672−2675.
(14) Balow, R. B.; Lundin, J. G.; Daniels, G. C.; Gordon, W. O.; McEntee, M.; Peterson, G. W.; Wynne, J. H.; Pehrsson, P. E. Environmental Effects on Zirconium Hydroxide Nanoparticles and Chemical Warfare Agent Decomposition: Implications of Atmospheric Water and Carbon Dioxide. *ACS Appl. Mater. Interfaces* **2017**, *9*, 39747−39757.
(15) Troya, D. Reaction Mechanism of Nerve-Agent Decomposition with Zr-Based Metal Organic Frameworks. *J. Phys. Chem. C* **2016**, *120*, 29312−29323.
(16) Plonka, A. M.; Wang, Q.; Gordon, W. O.; Balboa, A.; Troya, D.; Guo, W.; Sharp, C. H.; Senanayake, S. D.; Morris, J. R.; Hill, C. L.; Frenkel, A. I. In Situ Probes of Capture and Decomposition of Chemical Warfare Agent Simulants by Zr-Based Metal Organic Frameworks. *J. Am. Chem. Soc.* **2017**, *139*, 599−602.
(17) Wang, G.; Sharp, C.; Plonka, A. M.; Wang, Q.; Frenkel, A. I.; Guo, W.; Hill, C.; Smith, C.; Kollar, J.; Troya, D.; Morris, J. R. Mechanism and Kinetics for Reaction of the Chemical Warfare Agent Simulant, DMMP(g), with Zirconium(IV) MOFs: An Ultrahigh-Vacuum and DFT Study. *J. Phys. Chem. C* **2017**, *121*, 11261−11272.
(18) Nomiya, K.; Saku, Y.; Yamada, S.; Takahashi, W.; Sekiya, H.; Shinohara, A.; Ishimaru, M.; Sakai, Y. Synthesis and structure of dinuclear hafnium(IV) and zirconium(IV) complexes sandwiched between 2 mono-lacunary [small alpha]-Keggin polyoxometalates. *Dalton Trans.* **2009**, *28*, 5504−5511.
(19) Ly, H. G. T.; Absillis, G.; Parac-Vogt, T. N. Amide bond hydrolysis in peptides and cyclic peptides catalyzed by a dimeric Zr(iv)-substituted Keggin type polyoxometalate. *Dalton Trans.* **2013**, *42*, 10929−10938.
(20) Luong, T. K. N.; Absillis, G.; Shestakova, P.; Parac-Vogt, T. N. Solution Speciation of the Dinuclear ZrIV-Substituted Keggin Polyoxometalate $[\{\alpha\text{-}PW_{11}O_{39}Zr(\mu\text{-}OH)(H_2O)\}_2]^{8-}$ and Its Reactivity towards DNA-Model Phosphodiester Hydrolysis. *Eur. J. Inorg. Chem.* **2014**, *2014*, 5276−5284.
(21) Luong, T. K. N.; Absillis, G.; Shestakova, P.; Parac-Vogt, T. N. Hydrolysis of the RNA model substrate catalyzed by a binuclear ZrIV-substituted Keggin polyoxometalate. *Dalton Trans.* **2015**, *44*, 15690−15696.
(22) Luong, T. K. N.; Shestakova, P.; Mihaylov, T. T.; Absillis, G.; Pierloot, K.; Parac-Vogt, T. N. Multinuclear Diffusion NMR Spectroscopy and DFT Modeling: A Powerful Combination for Unraveling the Mechanism of Phosphoester Bond Hydrolysis Catalyzed by Metal-Substituted Polyoxometalates. *Chem. - Eur. J.* **2015**, *21*, 4428−4439.
(23) Luong, T. K. N.; Shestakova, P.; Absillis, G.; Parac-Vogt, T. N. Detailed Mechanism of Phosphoanhydride Bond Hydrolysis Promoted by a Binuclear ZrIV-Substituted Keggin Polyoxometalate Elucidated by a Combination of ^{31}P, ^{31}P DOSY, and ^{31}P EXSY NMR Spectroscopy. *Inorg. Chem.* **2016**, *55*, 4864−4873.
(24) Mihaylov, T. T.; Ly, H. G. T.; Pierloot, K.; Parac-Vogt, T. N. Molecular Insight from DFT Computations and Kinetic Measurements into the Steric Factors Influencing Peptide Bond Hydrolysis Catalyzed by a Dimeric Zr(IV)-Substituted Keggin Type Polyoxometalate. *Inorg. Chem.* **2016**, *55*, 9316−9328.
(25) Pope, M. T. 4.10 - Polyoxo Anions: Synthesis and Structure A2 - McCleverty. In *Comprehensive Coordination Chemistry II*; Meyer, T. J., Ed.; Pergamon: Oxford, England, 2003; pp 635−678.
(26) Hill, C. L. Introduction: Polyoxometalates Multicomponent Molecular Vehicles To Probe Fundamental Issues and Practical Problems. *Chem. Rev.* **1998**, *98*, 1−2.
(27) Lv, H.; Geletii, Y. V.; Zhao, C.; Vickers, J. W.; Zhu, G.; Luo, Z.; Song, J.; Lian, T.; Musaev, D. G.; Hill, C. L. Polyoxometalate water oxidation catalysts and the production of green fuel. *Chem. Soc. Rev.* **2012**, *41*, 7572−7589.
(28) Miras, H. N.; Yan, J.; Long, D.-L.; Cronin, L. Engineering polyoxometalates with emergent properties. *Chem. Soc. Rev.* **2012**, *41*, 7403−7430.
(29) Guo, W.; Lv, H.; Sullivan, K. P.; Gordon, W. O.; Balboa, A.; Wagner, G. W.; Musaev, D. G.; Bacsa, J.; Hill, C. L. Broad-Spectrum Liquid- and Gas-Phase Decontamination of Chemical Warfare Agents by One-Dimensional Heteropolyniobates. *Angew. Chem., Int. Ed.* **2016**, *55*, 7403−7407.
(30) Proust, A.; Matt, B.; Villanneau, R.; Guillemot, G.; Gouzerh, P.; Izzet, G. Functionalization and post-functionalization: a step towards polyoxometalate-based materials. *Chem. Soc. Rev.* **2012**, *41*, 7605−7622.
(31) Lauinger, S. M.; Yin, Q.; Geletii, Y. V.; Hill, C. L. Polyoxometalate Multi-Electron Catalysts in Solar Fuel Production. In *Advances in Inorganic Chemistry: Vol. 69. Polyoxometallate*

DOI: 10.1021/acscatal.8b00394
ACS Catal. 2018, 8, 7068−7076

Chemistry, 1st ed.; Cronin, L.; Eldik, R. v., Eds.; Elsevier, Oxford, England, 2017; pp 117−154.
(32) Li, J.; Güttinger, R.; Moré, R.; Song, F.; Wan, W.; Patzke, G. R. Frontiers of water oxidation: the quest for true catalysts. *Chem. Soc. Rev.* **2017**, *46*, 6124−6147.
(33) Weinstock, I. A.; Schreiber, R. E.; Neumann, R. Dioxygen in Polyoxometalate Mediated Reactions. *Chem. Rev.* **2018**, *118*, 2680−2717.
(34) Long, D.-L.; Tsunashima, R.; Cronin, L. Polyoxometalates: Building Blocks for Functional Nanoscale Systems. *Angew. Chem., Int. Ed.* **2010**, *49*, 1736−1758.
(35) Kato, C. N.; Shinohara, A.; Hayashi, K.; Nomiya, K. Syntheses and X-ray Crystal Structures of Zirconium(IV) and Hafnium(IV) Complexes Containing Monovacant Wells−Dawson and Keggin Polyoxotungstates. *Inorg. Chem.* **2006**, *45*, 8108−8119.
(36) Bassil, B. S.; Dickman, M. H.; Kortz, U. Synthesis and Structure of Asymmetric Zirconium-Substituted Silicotungstates, $[Zr_6O_2(OH)_4(H_2O)_3(\beta\text{-}SiW_{10}O_{37})_3]^{14-}$ and $[Zr_4O_2(OH)_2(H_2O)_4(\beta\text{-}SiW_{10}O_{37})_2]^{10-}$. *Inorg. Chem.* **2006**, *45*, 2394−2396.
(37) Carabineiro, H.; Villanneau, R.; Carrier, X.; Herson, P.; Lemos, F.; Ramôa Ribeiro, F.; Proust, A.; Che, M. Zirconium-Substituted Isopolytungstates: Structural Models for Zirconia-Supported Tungsten Catalysts. *Inorg. Chem.* **2006**, *45*, 1915−1923.
(38) Iijima, J.; Ishikawa, E.; Nakamura, Y.; Naruke, H. Synthesis and structural investigation of sandwich polyoxotungstates containing cerium (III/IV) and mono-lacunary Keggin tungstophosphate units. *Inorg. Chim. Acta* **2010**, *363*, 1500−1506.
(39) Lokeren, L. V.; Cartuyvels, E.; Absillis, G.; Willem, R.; Parac-Vogt, T. N. Phosphoesterase activity of polyoxomolybdates: diffusion ordered NMR spectroscopy as a tool for obtaining insights into the reactivity of polyoxometalate clusters. *Chem. Commun.* **2008**, 2774−2776.
(40) Steens, N.; Ramadan, A. M.; Absillis, G.; Parac-Vogt, T. N. Hydrolytic cleavage of DNA-model substrates promoted by polyoxovanadates. *Dalton Trans.* **2010**, *39*, 585−592.
(41) Vanhaecht, S.; Absillis, G.; Parac-Vogt, T. N. Hydrolysis of DNA model substrates catalyzed by metal-substituted Wells-Dawson polyoxometalates. *Dalton Trans.* **2012**, *41*, 10028−10034.
(42) Absillis, G.; Parac-Vogt, T. N. Peptide Bond Hydrolysis Catalyzed by the Wells−Dawson $Zr(\alpha_2\text{-}P_2W_{17}O_{61})_2$ Polyoxometalate. *Inorg. Chem.* **2012**, *51*, 9902−9910.
(43) Stroobants, K.; Moelants, E.; Ly, H. G. T.; Proost, P.; Bartik, K.; Parac-Vogt, T. N. Polyoxometalates as a Novel Class of Artificial Proteases: Selective Hydrolysis of Lysozyme under Physiological pH and Temperature Promoted by a Cerium(IV) Keggin-Type Polyoxometalate. *Chem. - Eur. J.* **2013**, *19*, 2848−2858.
(44) Stroobants, K.; Absillis, G.; Moelants, E.; Proost, P.; Parac-Vogt, T. N. Regioselective Hydrolysis of Human Serum Albumin by ZrIV-Substituted Polyoxotungstates at the Interface of Positively Charged Protein Surface Patches and Negatively Charged Amino Acid Residues. *Chem. - Eur. J.* **2014**, *20*, 3894−3897.
(45) Luong, T. K. N.; Shestakova, P.; Parac-Vogt, T. N. Kinetic studies of phosphoester hydrolysis promoted by a dimeric tetrazirconium(iv) Wells-Dawson polyoxometalate. *Dalton Trans.* **2016**, *45*, 12174−12180.
(46) Ly, H. G. T.; Mihaylov, T.; Absillis, G.; Pierloot, K.; Parac-Vogt, T. N. Reactivity of Dimeric Tetrazirconium(IV) Wells−Dawson Polyoxometalate toward Dipeptide Hydrolysis Studied by a Combined Experimental and Density Functional Theory Approach. *Inorg. Chem.* **2015**, *54*, 11477−11492.
(47) Ly, H. G. T.; Absillis, G.; Bajpe, S. R.; Martens, J. A.; Parac-Vogt, T. N. Hydrolysis of Dipeptides Catalyzed by a Zirconium(IV)-Substituted Lindqvist Type Polyoxometalate. *Eur. J. Inorg. Chem.* **2013**, *2013*, 4601−4611.
(48) Moon, S.-Y.; Proussaloglou, E.; Peterson, G. W.; DeCoste, J. B.; Hall, M. G.; Howarth, A. J.; Hupp, J. T.; Farha, O. K. Detoxification of Chemical Warfare Agents Using a Zr_6-Based Metal−Organic Framework/Polymer Mixture. *Chem. - Eur. J.* **2016**, *22*, 14864−14868.
(49) de Koning, M. C.; van Grol, M.; Breijaert, T. Degradation of Paraoxon and the Chemical Warfare Agents VX, Tabun, and Soman by the Metal−Organic Frameworks UiO-66-NH_2, MOF-808, NU-1000, and PCN-777. *Inorg. Chem.* **2017**, *56*, 11804−11809.
(50) Anderson, B. M.; Anderson, C. D. The Effect of Buffers on Nicotinamide Adenine Dinucleotide Hydrolysis. *J. Biol. Chem.* **1963**, *238*, 1475−1478.
(51) Hegg, E. L.; Burstyn, J. N. Hydrolysis of Unactivated Peptide Bonds by a Macrocyclic Copper(II) Complex: $Cu([9]aneN_3)Cl_2$ Hydrolyzes Both Dipeptides and Proteins. *J. Am. Chem. Soc.* **1995**, *117*, 7015−7016.
(52) Groves, J. T.; Baron, L. A. Models of zinc-containing proteases. Catalysis of cobalt(III)-mediated amide hydrolysis by a pendant carboxylate. *J. Am. Chem. Soc.* **1989**, *111*, 5442−5448.
(53) Miura, Y.-k.; Kamiya, Y. Highly Selective Sorption of Small Polar Molecules by a Nonporous Ionic Crystal of a Lacunary Keggin-type Heteropoly Anion and Alkali Metal Cations. *Chem. Lett.* **2012**, *41*, 331−333.
(54) Contant, R. Relations entre les tungstophosphates apparentés à l'anion $PW_{12}O_{40}^{3-}$. Synthèse et propriétés d'un nouveau polyoxotungstophosphate lacunaire $K_{10}P_2W_{20}O_{70}\bullet 24H_2O$. *Can. J. Chem.* **1987**, *65*, 568−573.
(55) Petříček, V.; Dušek, M.; Palatinus, L. Crystallographic Computing System JANA2006: General features. *Z. Kristallogr. - Cryst. Mater.* **2014**, *229*, 345.
(56) Bowers, G. N.; McComb, R. B.; Christensen, R. G.; Schaffer, R. High-purity 4-nitrophenol: purification, characterization, and specifications for use as a spectrophotometric reference material. *Clinical Chemistry* **1980**, *26*, 724−729.
(57) Gasparro, F. P.; Kolodny, N. H. NMR determination of the rotational barrier in N,N-dimethylacetamide. A physical chemistry experiment. *J. Chem. Educ.* **1977**, *54*, 258.
(58) Gutz, I. G. R. CurTiPot − pH and Acid−Base Titration Curves: Analysis and Simulation freeware. http://www.iq.usp.br/gutz/Curtipot_.html (accessed November 14, 2016).
(59) Islamoglu, T.; Ortuño, M. A.; Proussaloglou, E.; Howarth, A. J.; Vermeulen, N. A.; Atilgan, A.; Asiri, A. M.; Cramer, C. J.; Farha, O. K. Presence versus Proximity: The Role of Pendant Amines in the Catalytic Hydrolysis of a Nerve Agent Simulant. *Angew. Chem., Int. Ed.* **2018**, *57*, 1949−1953.
(60) Sullivan, K. P.; Neiwert, W. A.; Zeng, H.; Mehta, A. K.; Yin, Q.; Hillesheim, D. A.; Vivek, S.; Yin, P.; Collins-Wildman, D. L.; Weeks, E. R.; Liu, T.; Hill, C. L. Polyoxometalate-based gelating networks for entrapment and catalytic decontamination. *Chem. Commun.* **2017**, *53*, 11480−11483.

DOI: 10.1021/acscatal.8b00394
ACS Catal. 2018, 8, 7068−7076